Physics-informed Probability Distribution Assessment for Primary Frequency Regulation Capability of Wind Farms Considering Wind Speed Uncertainty

Wenlong Wu, Zhongguan Wang, *Member*, *IEEE*, Xialin Li, *Member*, *IEEE*, Li Guo, *Member*, *IEEE*, Yixin Liu, Jiaqing Zhai, and Chengshan Wang, *Senior Member*, *IEEE*

***Abstract*—High penetration of wind power into power grids deteriorates system frequency stability. Wind turbines (WTs) are required by grid codes to participate in primary frequency regulation (PFR) by adjusting their rotor speed to utilize the stored kinetic energy. However, frequency support causes a change in rotor speed, and hence, the PFR capability of a wind farm is limited by a time-varying boundary. As the mechanical transient process of the WT is determined by wind speed, it is necessary to forecast the PFR capability of wind farms based on wind speed distribution, to arrange the system scheduling plan while considering dynamic safety. In this paper, a physics-informed probability distribution assessment method is proposed for the PFR capability of wind farms considering wind speed uncertainty. Constructing the analytical correlation relationship between state variables based on Koopman-operator-theory-based state space transformation, the probability density function of the maximum feasible droop coefficient of a wind farm is derived based on the wind speed probability distribution. The simulation results demonstrate that the proposed method achieves a five-order-of-magnitude reduction in computational time compared with the Monte Carlo and time-domain simulation methods, and possesses the advantages of independence from physical parameters and random sampling errors, as well as a simple analytical expression of the probability distribution of PFR capability.**

***Index Terms*—Droop control, frequency regulation, probabilistic forecast, probability distribution, state space transformation, wind farm, wind speed, uncertainty.**

I. Introduction

With the increasing penetration of wind power into power grids, system dynamics caused by frequency oscillations have drawn much attention [1], [2]. When variable-speed wind turbines (WTs) are connected to the power grid via power electronic devices, their rotor speed is decoupled from the system frequency [3], [4]. In legacy mode, WTs typically operate in a maximum power point tracking manner [5] and do not provide additional power backup to respond to changes in system frequency. This inevitably leads to a decrease in the system inertia and frequency stability. Furthermore, wind power generation is significantly influenced by meteorological factors such as wind speed [6]. The uncertainty in wind speed results in fluctuations in the power output from wind farms, further deteriorating the dynamic characteristics of the system [7].

To satisfy the grid codes, wind farms are required to participate in system primary frequency regulation (PFR) by emulating the droop characteristics of the thermal units [8]-[10]. Owing to the regulation of the converter power output, changes in the rotor speed are a consequence of the release of stored kinetic energy to respond to frequency variations [11]. As the rotor speed should be maintained within the security boundary to prevent WTs from tripping, it is important to appropriately distribute the power reference to the WTs through PFR control [12]. In our previous studies [13]-[15], a state-of-energy (SOE) index is utilized to optimize the power distribution among WTs, which changes the rotor speed of different WTs in synchronization, fully exploiting the maximum PFR capability of wind farms.

The frequency support capability, that is, the maximum droop coefficients that wind farms can provide, varies with different wind speed conditions. To ensure the safety of the rotor speed during the PFR process, an assessment of the PFR boundary based on wind speed forecasts is necessary for both wind farms and the system, particularly in a low-inertia system, where the operators should utilize the results to make scheduling plans. Only operational costs under power balance constraints [16], [17] are considered in the classical

Manuscript received: December 16, 2024; revised: March 25, 2025; accepted: May 30, 2025. Date of CrossCheck: May 30, 2025. Date of online publication: July 7, 2025.

This work was supported in part by the National Key R&D Project (No. 2023YFB2406700), in part by the Specific Research Fund of the Innovation Platform for Academicians of Hainan Province (No. YSPTZX202305), and in part by the National Natural Science Foundation of China (No. U23B20123).

W. Wu, Z. Wang (corresponding author), X. Li, L. Guo, Y. Liu, J. Zhai, and C. Wang are with the School of Electrical and Information Engineering, Tianjin University, Tianjin, China (e-mail: 2023234404@tju.edu.cn; wang_zg@tju.edu.cn; xialinlee@tju.edu.cn; liguo@tju.edu.cn; liuyixin@tju.edu.cn; zhaijiaqing@tju.edu.cn; cswang@tju.edu.cn).

DOI: 10.35833/MPCE.2024.001345

unit commitment and economic dispatch problems. However, with the increasing penetration of renewable power generation and the decreasing inertia provided by thermal units, dynamic frequency security should also be considered [18]. Reference [19] constructs frequency security constraints in the unit commitment model and develops the concept of frequency stabilization margin. However, existing scheduling schemes neglect the time-dependent characteristics of the PFR capabilities of wind farms. Therefore, by considering rotor speed constraints and wind speed uncertainty, the online forecast of PFR capability plays a crucial role in the operation of power systems with a high penetration of renewable power generation.

By solving a dynamic optimization model with nonlinear electromechanical transient differential equations, the PFR capability of wind farms can be calculated from the perspective of the mechanism. In [20], an assessment method for the PFR capability of wind farms based on the available reserves and current wind speed is proposed. Reference [21] constructs a system frequency response model for a power system with a high penetration of wind power and simplifies the process of solving for control parameters such as the droop coefficient. However, the aforementioned methods are based on the traditional large-scale time-domain dynamic model, which may encounter challenges when being solved analytically. Time-domain simulations suffer from heavy computations, making it difficult to track rapid changes in wind speed. Moreover, the assessment performance is heavily dependent on the accuracy of the physical parameters, making it inapplicable to actual conditions with significant errors.

A simplified solution for complicated physical models is a distinct advantage of data-driven approaches. By utilizing the historical PFR data of wind farms for data-driven training, it is possible to establish a correlation model between the wind speed and maximum PFR coefficient. An artificial neural network is developed in [22] to train the PFR strategy and ensure that the droop coefficient is within the security range. In [23], a multi-intelligent deep learning reinforcement algorithm is used to optimize the parameters of a WT controller for a favorable frequency response of a wind farm. In our previous study [24], a dimension-augmented linear model of the rotor speed based on a data-driven state space transformation is proposed to assess the maximum coefficient. Despite the simplified solution process, the aforementioned data-driven assessment methods rely on deterministic wind speeds measured in real time. To arrange the system unit commitment and scheduling plan in advance and prevent frequency instability, it is necessary to pre-characterize the boundary of the PFR capability of wind farms based on wind speed forecasts.

Nevertheless, uncertainty is an inherent property of wind speed forecasts. Based on a point forecast of wind speed, the PFR capability is likely to deviate from the actual situation. In fact, state-of-the-art wind speed forecasts usually exhibit a probability distribution [25]; thus, the maximum droop coefficients assessed according to the wind speed should also follow a certain distribution. In theory, by utilizing time-domain simulation combined with the Monte Carlo simulation method, the probability distribution of the maximum droop coefficient of a wind farm can be fitted based on mathematical regression [26]; however, the computational time cost is extremely high, and the exact probability density expression is still beyond the reach of statistical methods.

Therefore, to construct the probability density function (PDF) of the maximum feasible droop coefficient of a wind farm, this paper presents a physics-informed probability distribution assessment method that utilizes historical data to obtain a dimension-augmented correlation model of the rotor speed, wind speed, and droop coefficient. In addition, we derive an exact expression for the PDF of the maximum droop coefficient based on wind speed forecasts. The main contributions of this study are as follows.

1) A physics-informed probability distribution assessment method for PFR capability is developed, where the PFR mechanism of wind farms is embedded within a dimension-augmented correlation model, making it independent of the accuracy of physical parameters and vastly improving the computational efficiency over Monte Carlo simulation methods.

2) An analytical expression of the probability distribution between the PFR capability and wind speed is derived based on the dimension-augmented correlation model, with the advantage of immunity to sampling errors.

3) A uniform and simple probability distribution of the maximum droop coefficient and expected final rotor speed is provided, which contributes to creating a unit commitment and scheduling plan in advance for the system operator.

The remainder of this paper is organized as follows. Section II describes the mechanism model for the PFR capability assessment considering the rotor speed constraint. Section III derives the probability distributions of the wind speed forecast based on the Weibull distribution and the PFR capability. Section IV presents the probability distribution of the PFR capability based on the Koopman operator theory. Section V presents case studies to verify the performance of the proposed method. Finally, Section VI concludes this paper.

II. Mechanism Model for PFR Capability Assessment Considering Rotor Speed Constraint

A. Electromechanical Transient Model of WTs

To assess the aggregated PFR capability of a wind farm, it is necessary to conduct a mechanistic analysis to construct an electromechanical transient model for WTs. In this study, a WT with a full-scale power converter is taken as the analytic target, and its structure is shown in Fig. 1, where ω is the rotor speed; f is the real-time frequency; P_{ref} is the reference active power output; and PWM is the pulse width modulation. Note that the proposed method is applicable to all WTs with power control mechanisms based on rotor kinetic energy regulation.

The mechanical power captured by WT blades can be expressed as:

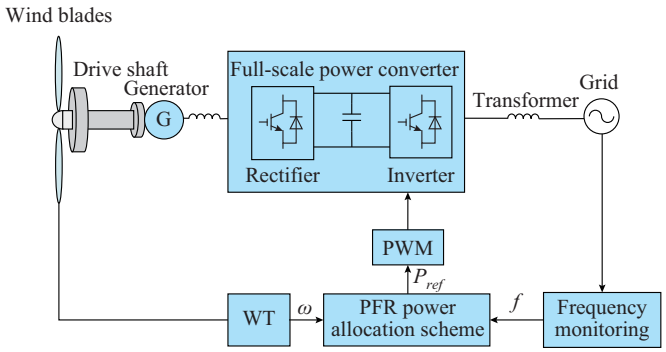

Fig. 1. Structure of a WT with a full-scale power converter.

$$P_{m,i}=\frac{1}{2}\rho S v_i^3 C_{p,i}(\lambda_i,\beta_i) \tag{1}$$

where $P_{m,i}$ is the mechanical power captured by the blades of the i^{th} WT; ρ is the air density; S is the swept area of the blades; v_i is the real-time wind speed of the i^{th} WT; and $C_{p,i}(\lambda_i,\beta_i)$ is the capture coefficient of the i^{th} WT, which can be expressed as:

$$\begin{cases} C_{p,i}(\lambda_i,\beta_i)=0.22\left(\dfrac{116}{\lambda_1}-0.4\beta_i-5\right)\mathrm{e}^{\frac{-12.5}{\lambda_1}} \\ \lambda_i=\dfrac{R\omega_i}{v_i} \\ \dfrac{1}{\lambda_1}=\dfrac{1}{\lambda_i+0.08\beta_i}-\dfrac{0.035}{\beta_i^3+1} \end{cases} \tag{2}$$

where λ_i is the ratio of the blade tip speed to the wind speed; β_i is the pitch angle of the i^{th} WT; R is the blade radius; and ω_i is the rotor speed of the i^{th} WT.

During the PFR process, a mismatch between the mechanical and electromagnetic torques causes a change in the WT rotor speed:

$$\dot{\omega}_i=\frac{1}{J_c}(T_{m,i}-T_{e,i})=\frac{1}{J_c}\left(\frac{P_{m,i}}{\omega_i}-\frac{P_{e,i}}{\omega_i}\right) \tag{3}$$

where $\dot{\omega}_i$ is the rate of change in the rotor speed; J_c is the rotational inertia; $T_{m,i}$ is the mechanical torque of the i^{th} WT; $T_{e,i}$ is the electromagnetic torque of the i^{th} WT; and $P_{e,i}$ is the electromagnetic power of the i^{th} WT.

B. Optimal PFR Power Allocation Scheme of WTs Considering Rotor Speed

In the PFR process, the change in the WT rotor speed is determined by the PFR power allocation scheme in the wind farm. Considering the initial state differences between WTs, each WT should share the PFR power in proportion to its SOE. This scheme can fully utilize all the WTs in the wind farm while maintaining synchronized speed changes, thus maximizing the aggregated droop coefficient of the wind farm. Note that this study mainly focuses on the assessment of the PFR capability, and the control methodology to achieve fast power allocation in the PFR process can be found in our previous studies [14], [15].

The kinetic energy stored in the blades of the i^{th} WT can be expressed as:

$$E_i=\frac{1}{2}J_c\omega_i^2 \tag{4}$$

Given the security range of the rotor speed, the SOE of the i^{th} WT can be expressed as:

$$SOE_i=\begin{cases} (E_i-E_{\min,i})/(E_{\max,i}-E_{\min,i})= \\ \quad(\omega_i^2-\omega_{\min,i}^2)/(\omega_{\max,i}^2-\omega_{\min,i}^2) \quad f<f_n \\ (E_{\max,i}-E_i)/(E_{\max,i}-E_{\min,i})= \\ \quad(\omega_{\max,i}^2-\omega_i^2)/(\omega_{\max,i}^2-\omega_{\min,i}^2) \quad f\geq f_n \end{cases} \tag{5}$$

where $E_{\max,i}$ and $E_{\min,i}$ are the upper and lower limits of the stored energy, respectively; $\omega_{\max,i}$ and $\omega_{\min,i}$ are the upper and lower limits of the rotor speed, respectively; and f_n is the nominal frequency. The value range of SOE_i is from 0 to 1, and a larger value indicates that the WT has a wider adjustable range when frequency drops and is responsible for undertaking more unbalanced power.

To balance the PFR power of the WTs, the difference between mechanical and electromagnetic power is designed to be proportional to SOE_i, which satisfies:

$$\frac{P_{m,i}-P_{e,i}}{SOE_i}=\frac{P_{m,j}-P_{e,j}}{SOE_j} \quad i,j\in\{1,2,\ldots,l\} \tag{6}$$

where l is the number of WTs.

C. PFR Capability Assessment Model of Wind Farms

In the case of a significant frequency change, the wind farm, as an independent participant, needs to adjust its active power output to maintain system frequency stability. This process is achieved by emulating the power-frequency static characteristics of synchronous units during the PFR:

$$\Delta P_{WF}=K_f(f_n-f) \tag{7}$$

where ΔP_{WF} is the PFR power of the wind farm; and K_f is the droop coefficient of the wind farm.

According to (6), the electromagnetic power of the i^{th} WT can be expressed as:

$$P_{e,i}=K_f(f_n-f)\cdot SOE_i\Big/\sum_{i=1}^{l}SOE_i+P_{m,i} \tag{8}$$

Based on the center-of-inertia assumption, the external system can be approximated as a first-order inertial element:

$$\dot{f}=\frac{f_n}{2H}[P_0+P_G-P_L+(K_G+K_f)(f_n-f)] \tag{9}$$

where $\dot{f}$ is the rate of change in the frequency; H is the system inertia coefficient; P_0 is the initial active power of the wind farms; P_G is the initial active power of the synchronous units; P_L is the system load; and K_G is the droop coefficient of the synchronous units.

In this study, the PFR capability assessment is equivalent to calculating the maximum droop coefficient $K_{f,\max}$ of the wind farm. In addition to constraints (1)-(3), (8), and (9), bound constraints are considered to ensure that the rotor speed remains within the safety range. Therefore, PFR capability assessment is a dynamic optimization problem involving high-order nonlinear differential-algebraic equations, which are difficult to solve analytically. Typically, a dynamic model is converted into an algebraic equation through discretization. Therefore, a complete discrete algebraic PFR capability assessment model is constructed as:

$$\max K_f \tag{10a}$$

s.t.

$$\omega_i(t+1)=\frac{T(P_{m,i}(t)-P_{e,i}(t))}{J_c\omega_i(t)}+\omega_i(t) \tag{10b}$$

$$P_{m,i}(t)=\frac{1}{2}\rho S v_i^3 C_{p,i}(\lambda_i(t),\beta_i) \tag{10c}$$

$$SOE_i(t)=\begin{cases}\dfrac{\omega_i^2(t)-\omega_{\min,i}^2}{\omega_{\max,i}^2-\omega_{\min,i}^2} & f(t)<f_n\\ \dfrac{\omega_{\max,i}^2-\omega_i^2(t)}{\omega_{\max,i}^2-\omega_{\min,i}^2} & f(t)\geq f_n\end{cases} \tag{10d}$$

$$P_{e,i}(t)=K_f(f_n-f(t))\cdot SOE_i(t)\Big/\sum_{i=1}^{l}SOE_i(t)+P_{m,i}(t) \tag{10e}$$

$$f(t+1)=f(t)+\frac{f_nT}{2H}[P_0+P_G-P_L+(K_G+K_f)(f_n-f(t))] \tag{10f}$$

$$\omega_{\min,i}\leq\omega_i(t)\leq\omega_{\max,i} \tag{10g}$$

where $i,j\in\{1,2,\ldots,l\}$; t is the time step; and T is the time interval.

Note that the discrete assessment model (10) remains a complex problem with nonlinear algebraic equations, which is unsuitable for rapid calculation under time-varying conditions.

In addition, it is necessary for the system operator to forecast the PFR capability of all wind farms in a day-ahead manner to create a frequency-characteristic scheduling plan. However, actual wind speeds typically do not exactly match point-forecast results. Instead, they exhibit a probability distribution around the point. Therefore, in the forecast stage, PFR capability should also be considered as a random variable with a probability distribution. By using model (10), it is difficult to obtain the PDF of $K_{f,\max}$ because there is no explicit correlation between the wind speed and maximum PFR capability.

III. Probability Distributions of Wind Speed Forecast Based on Weibull Distribution and PFR Capability

A. Probability Distribution of Wind Speed Forecast Based on Weibull Distribution

Traditional wind speed forecast relies on deterministic point or interval prediction models based on historical data, which involve only limited information and cannot depict uncertainty. To address this drawback, recent studies have focused on the development of probabilistic models to estimate the uncertainty in wind speed forecast. For example, probabilistic prediction methods based on the Weibull distribution are widely adopted. The Weibull PDF is used to describe the wind speed distribution and proves to provide satisfactory accuracy [27]-[29].

The PDF and cumulative density function (CDF) of the Weibull distribution are given by:

$$f_{weibull}(v,s,k)=\begin{cases}\dfrac{k}{s}\left(\dfrac{v}{s}\right)^{k-1}\mathrm{e}^{-\left(\frac{v}{s}\right)^k} & v\geq 0\\ 0 & v<0\end{cases} \tag{11}$$

$$F_{weibull}(v,s,k)=\begin{cases}1-\mathrm{e}^{-\left(\frac{v}{s}\right)^k} & v\geq 0\\ 0 & v<0\end{cases} \tag{12}$$

where v is the wind speed variable; s is the scale parameter; and k is the shape parameter.

Based on the PDF of the wind speed forecast, the PDF of the maximum PFR capability can be obtained through a Monte Carlo simulation combined with model (10). The procedure is described as follows.

1) Given a PDF of wind speeds, perform random sampling based on the probability distribution.

2) Substitute the sampled points into model (10), and use time-domain simulation to calculate a PFR capability point.

3) Repeat wind speed sampling and obtain a scatter distribution of $K_{f,\max}$.

4) Divide the scattered points into small intervals to count the occurrences in each interval and generate a distribution histogram.

5) Use kernel density estimation to obtain the PDF of $K_{f,\max}$.

Note that the calculation process of the PDF of the PFR capability is nonanalytic and suffers from an unacceptable computational time. Moreover, the results are significantly affected by random errors in the sampling points. To address this problem, this paper proposes a physics-informed probability distribution assessment method for PFR capability of wind farms based on the Koopman operator theory, which directly provides a correlation expression between $K_{f,\max}$ and wind speed, thus rapidly generating an accurate PDF of the PFR capability.

B. Probability Distribution of PFR Capability

When participating in the PFR, the rotor speed changes during the process. By setting the expected final rotor speed, denoted as ω_{final}, the droop coefficient of the wind farm, denoted as K_f^*, can be determined. If ω_{final} is set to be the speed limit of the WT, denoted as ω_{lim}, the expression for $K_{f,\max}$ can be obtained by solving (10).

To derive the expression for the PDF of K_f^*, the CDF should first be calculated, which can be expressed as:

$$F(x)=\Pr\{K_f^*\leq x\} \tag{13}$$

where x denotes the function variable of the CDF.

Note that, with a determined ω_{final} for WTs, K_f^* is negatively correlated with the wind speed when the system frequency increases. Conversely, it is positively correlated with the wind speed when the system frequency decreases. Therefore, the droop coefficient of wind farm and the wind speed exhibit a monotonic relationship, as shown in Fig. 2.

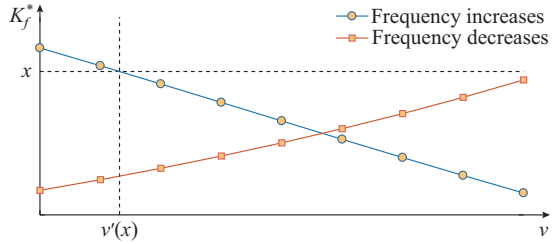

Fig. 2. Relationship between droop coefficient of wind farm and wind speed.

Thus, the CDF of K_f^* can be rewritten as (14) when the system frequency increases.

$$F(x)=\Pr\{K_f^*\le x\}=\Pr\{v\ge v'(x)\} \tag{14}$$

where $v'(x)$ is the wind speed when K_f^* takes the value of x. Thus, the calculation of the CDF is transformed from solving the probability value of K_f^* to v.

The wind speed follows a Weibull distribution for which the PDF is explicit. Thus, we only need to determine each $v'(x)$ corresponding to a different x, and the CDF can be obtained as:

$$F(x)=\Pr\{K_f^*\le x\}=\Pr\{v\ge v'(x)\}=1-F_{weibull}(v'(x)) \tag{15}$$

As discussed in Section II, wind speed can be expressed as a function of K_f^* and ω_{final}, namely,

$$v=\phi_u(\omega_{final},K_f^*) \tag{16}$$

where ϕ_u is the function of wind speed expressed in terms of the final rotor speed and PFR coefficient as the frequency increases. Replacing K_f^* with x yields:

$$v'(x)=\phi_u(\omega_{final},x) \tag{17}$$

Substituting (17) into (15) yields the final expression for the CDF:

$$F(x)=1-F_{weibull}(\phi_u(\omega_{final},x)) \tag{18}$$

Hence, the PDF of K_f^* can be expressed as:

$$f(x)=-f_{weibull}(\phi_u(\omega_{final},x))\frac{\delta\phi_u(\omega_{final},x)}{\delta x} \tag{19}$$

Similarly, when the system frequency decreases, the CDF can be written as:

$$\begin{aligned}F(x)&=\Pr\{K_f^*\le x\}=\Pr\{v\le v'(x)\}=\\&F_{weibull}(v'(x))=F_{weibull}(\phi_d(\omega_{final},x))\end{aligned} \tag{20}$$

where ϕ_d is the function of the wind speed expressed in terms of the final rotor speed and PFR coefficient as the frequency decreases.

Hence, the PDF of K_f^* can be expressed as:

$$f(x)=f_{weibull}(\phi_d(\omega_{final},x))\frac{\delta\phi_d(\omega_{final},x)}{\delta x} \tag{21}$$

In summary, the PDF of K_f^* can be summarized as:

$$f(x)=\begin{cases}-f_{weibull}(\phi_u(\omega_{final},x))\dfrac{\delta\phi_u(\omega_{final},x)}{\delta x} & f\ge f_n\\ f_{weibull}(\phi_d(\omega_{final},x))\dfrac{\delta\phi_d(\omega_{final},x)}{\delta x} & f<f_n\end{cases} \tag{22}$$

By using $\omega_{final}=\omega_{lim}$, the PDF of the maximum droop coefficient $K_{f,\max}$ can be obtained.

Based on the derivation above, we establish a probabilistic mapping relationship between the wind speed and the PFR capability, which is illustrated in Fig. 3.

However, on the one hand, the correlation among the wind speed, final rotor speed, and PFR coefficient, i.e., $v=\phi(\omega_{final},K_f^*)$, is difficult to express explicitly according to (10). On the other hand, an analytical model, as opposed to a statistical curve, is significant for the subsequent scheduling plan. To address this issue, this paper proposes a physics-informed assessment method based on the Koopman operator theory. This model is trained with the historical data of the PFR capacity of wind farms to obtain a functional expression for the correlation of rotor speed, droop coefficient, and wind speed.

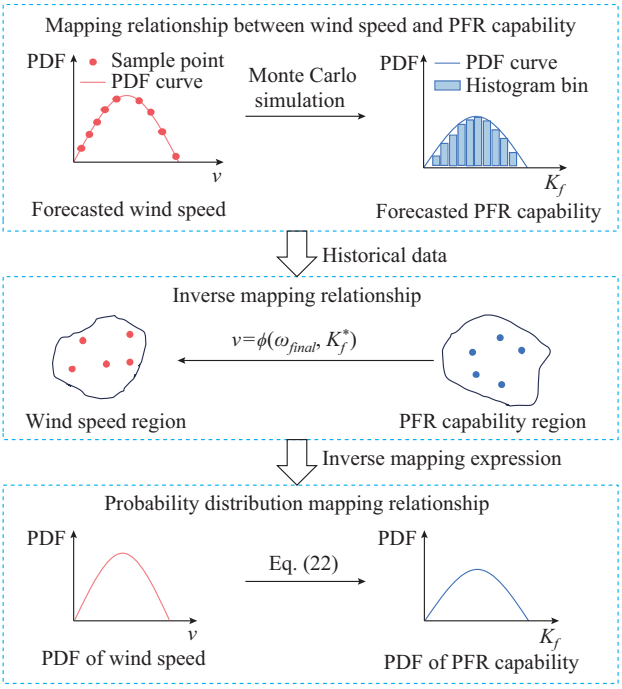

Fig. 3. Probabilistic mapping relationship between wind speed and PFR capability.

IV. Probability Distribution of PFR Capability Based on Koopman Operator Theory

A. Koopman-operator-theory-Based State Space Transformation

The essence of the Koopman operator theory is that, by augmenting the dimension of input variables, a nonlinear algebraic model in a low-dimensional space can be converted into a linear form in a high-dimensional Hilbert space without loss of accuracy [30]-[32].

Considering the wind speed of wind farms as the output variable and the expected final rotor speed of WTs and the droop coefficient as input variables, the PFR model $v=\phi(\omega_{final},K_f^*)$ exhibits complex nonlinear characteristics. Based on using the dimension-augmenting space transformation, there exists a linear relationship matrix $\boldsymbol{M}$, by which the original PFR model can be expressed as:

$$v=\boldsymbol{M}\boldsymbol{X}_{lift}=[\boldsymbol{M}_1\quad\boldsymbol{M}_2]\begin{bmatrix}\boldsymbol{X}\\ \boldsymbol{\psi}(\boldsymbol{X})\end{bmatrix} \tag{23}$$

where $\boldsymbol{M}$ is the data-driven linear relationship matrix; $\boldsymbol{X}_{lift}$ is the matrix of augmented input variables; $\boldsymbol{M}_1$ and $\boldsymbol{M}_2$ are the block matrix elements of $\boldsymbol{M}$; $\boldsymbol{X}$ is the vector of input variables, namely, K_f^* and ω_{final}; and $\boldsymbol{\psi}(\boldsymbol{X})$ is the dimension-augmenting function of the input variables. In theory, linear expression (23) is strictly equivalent to the original nonlinear relationship only when the augmented dimension is infinite. However, in practice, augmenting the dimensions to an appropriate number is sufficient to obtain a high-precision approximation.

Assuming that the dimension of input variables is m, the j^{th} dimension-augmenting function is given as:

$$\psi_j(\boldsymbol{X}) = h(\boldsymbol{X} - \boldsymbol{c}_j) \tag{24}$$

where $\boldsymbol{c}_j$ is the j^{th} base vector, whose elements are random within the variable range of input variables; and $h(\cdot)$ is the intermediate function. Considering the complex nonlinearity of the original PFR model, it is important to choose an appropriate dimension-augmenting function. In this study, a "polyharmonic" function is adopted, whose j^{th} function is given as:

$$\begin{cases} h_b(\boldsymbol{X} - \boldsymbol{c}_j) = \sqrt{\sum_{i=1}^{m} (X_i - c_{ji})} \\ h(\boldsymbol{X} - \boldsymbol{c}_j) = h_b(\boldsymbol{X} - \boldsymbol{c}_j) \cdot \lg h_b(\boldsymbol{X} - \boldsymbol{c}_j) \end{cases} \tag{25}$$

where $h_b(\cdot)$ is the basis function; X_i is the i^{th} element in $\boldsymbol{X}$; and c_{ji} is the i^{th} element in $\boldsymbol{c}_j$.

The data-driven linear relationship matrix $\boldsymbol{M}$ can be trained using the historical PFR data from a wind farm. Assuming that the number of historical data samples is S, the training set for input variables $\boldsymbol{\chi}$ and the training set for output variables $\boldsymbol{\gamma}$ can be expressed as:

$$\begin{cases} \boldsymbol{\chi} = [\boldsymbol{X}_1, \boldsymbol{X}_2, \ldots, \boldsymbol{X}_i, \ldots, \boldsymbol{X}_S] \\ \boldsymbol{\gamma} = [\boldsymbol{Y}_1, \boldsymbol{Y}_2, \ldots, \boldsymbol{Y}_i, \ldots, \boldsymbol{Y}_S] \end{cases} \tag{26}$$

where $\boldsymbol{X}_i$ is the i^{th} historical data sample for input variables; and $\boldsymbol{Y}_i$ is the i^{th} historical data sample for output variables. In addition, the training set for augmented input variables is expressed as:

$$\boldsymbol{\chi}_{lift} = [\boldsymbol{X}_{lift,1}, \boldsymbol{X}_{lift,2}, \ldots, \boldsymbol{X}_{lift,i}, \ldots, \boldsymbol{X}_{lift,S}] \tag{27}$$

where $\boldsymbol{X}_{lift,i}$ is the i^{th} sample for augmented input variables.

Based on historical data, the linear matrix $\boldsymbol{M}$ can be estimated using the least-squares method as:

$$\boldsymbol{M} = \boldsymbol{\gamma}\boldsymbol{\chi}_{lift}^{\mathrm{T}} [\boldsymbol{\chi}_{lift} \boldsymbol{\chi}_{lift}^{\mathrm{T}}]^{\dagger} \tag{28}$$

where $[\cdot]^{\dagger}$ denotes the Moore-Penrose inverse of the matrix.

Thus, the data-driven linear relationship (23) is obtained, which can be substituted for the original implicit relationship in the analytical expression of PDF (22). Note that the Koopman-operator-theory-based method generates a global linear model, and hence, it is unnecessary for the training set to cover extreme scenarios of PFR.

With the PDF of the maximum droop coefficient $K_{f,\max}$, the upper confidence interval of $K_{f,\max}$ with a confidence level α, denoted as $K_{f,\max,\alpha}$, can be analytically calculated as:

$$\Pr\{K_{f,\max} \geq K_{f,\max,\alpha}\} = \alpha \tag{29}$$

The wind farm can be considered to have an α probability of providing a maximum PFR droop coefficient of no less than $K_{f,\max,\alpha}$ with the forecasted wind speed probability distribution. The results provide a reference value for droop coefficient prediction from a probabilistic perspective, which is of considerable significance in dynamic characteristic optimization.

B. Overall Process of Probabilistic Forecast for PFR Capability of Wind Farms

The overall process of probabilistic forecast for the PFR capability of wind farms can be divided into two stages: offline training and online prediction.

The offline training process consists of the following steps. ① Obtain the historical PFR data of the wind farm, including v, K_f^*, and ω_{final}. ② Normalize the training set, determine the base vectors $\boldsymbol{c}_j$, and calculate $\boldsymbol{X}_{lift}$. ③ Train the matrix $\boldsymbol{M}$ using the least-squares method.

The online prediction process includes the following steps. ① Obtain the Weibull distribution parameters of the wind speed for the wind farm. ② Calculate the PDF of the droop coefficients according to different ω_{final}. ③ Based on the PDF of the maximum droop coefficient of the wind farm obtained from $\omega_{final} = \omega_{lim}$, calculate $K_{f,\max,\alpha}$ with an α confidence level, and report the results to the system operator. ④ If the predicted wind speed distribution changes, repeat ①-③ and update the probability distribution of the maximum droop coefficient in real time.

Note that, as the data-driven training process proposed herein is conducted offline, the coefficient matrix in the online prediction stage only needs to be retrained when the static parameters of the wind farm change. During the online operation of a wind farm, the continuous input of new data is not required to optimize the linear evaluation model. The overall process of probabilistic forecast for the PFR capability of wind farms is shown in Fig. 4.

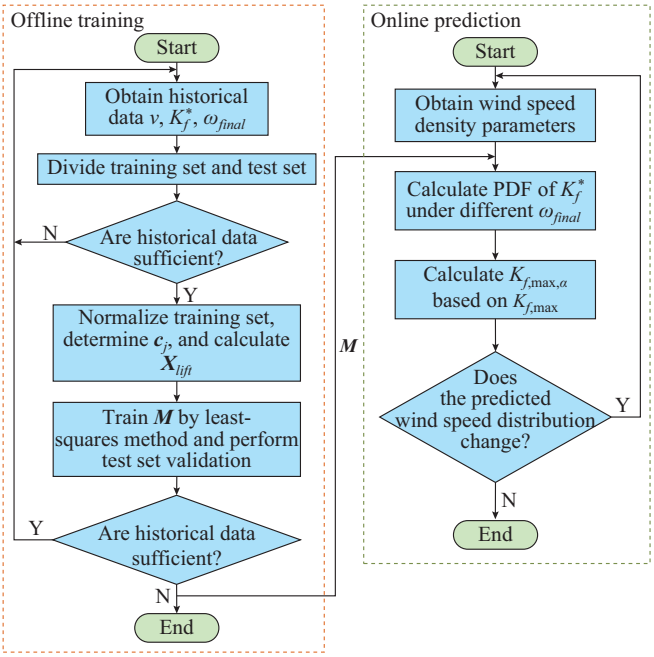

Fig. 4. Overall process of probabilistic forecast for PFR capability of wind farms.

V. Case Study

This section presents a simulation to demonstrate the performance of the proposed method. For comparison, simulation a time-domain simulation combined with the Monte Carlo simulation method is used to validate the results. In the test system, the wind farm comprises 16 WTs, and the rated capacity of each WT is 4 MW. The security range of the rotor speed is set to be [0.7, 1.44]p.u., and the training set of the droop coefficient covers $K_f^* \in [0, 50]$MW/Hz for the fre-

quency-rising scenario and $K_f^* \in [0, 35]$MW/Hz for the frequency-dropping scenario. The wind speed for training is $v \in [5, 12]$m/s, which covers the most typical wind speed scenarios encountered in wind farm operations. Owing to the global linearization advantage of the Koopman operator theory, there is no need for the final rotor speed range in the training set to cover extreme PFR scenarios, and it is therefore set to be [0.76, 1.38]p.u.. The number of augmented dimensions for input variables is 1500, which ensures sufficient accuracy within an acceptable computational time. The probability distributions of wind speed forecasts for four different time periods t_1-t_4 in the wind farm are generated, as shown in Fig. 5. Without loss of generality, the proposed method is first tested by considering time period t_1 as a typical scenario.

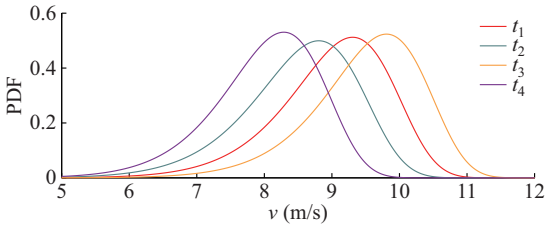

Fig. 5. Probability distributions of wind speed forecasts for four different time periods in wind farm.

A. Accuracy Analysis of Data-driven Model

As mentioned previously, the trained linear relationship is strictly equivalent to the original nonlinear relationship $v = \phi(\omega_{final}, K_f^*)$ only when the augmented dimension is infinite. In practice, the number of augmented dimensions must be appropriately selected to ensure good performance.

Load fluctuations are simulated to activate the PFR process and obtain the historical PFR data. The frequency-rising and frequency-dropping scenarios are discussed separately. To validate the accuracy of the trained linear model $v = \phi(\omega_{final}, K_f^*)$, we evaluate both scenarios of the test set. In the frequency-rising scenario, the expected final rotor speeds are 1.38 p.u., 1.40 p.u., 1.42 p.u., and 1.44 p.u., respectively, and for the frequency-dropping scenario, the expected final rotor speeds are 0.76 p.u., 0.74 p.u., 0.72 p.u., and 0.7 p.u., respectively. With different given droop coefficients, the wind speed corresponding to the expected rotor speeds can be calculated using a data-driven dimension-augmented correlation model or obtained using a time-domain simulation. The results from the proposed method are compared with those of the time-domain simulation to demonstrate accuracy, and the relative errors are shown in Fig. 6. Note that the rotor speed training range for the test cases is [0.76, 1.38]p.u.; however, the test cases still demonstrate good accuracy even outside this range, further validating the advantages of the Koopman operator theory in global linearization.

The assessment results of K_f^* are sufficiently close to those of the time-domain simulation, where the maximum error is within 3%. To further verify the accuracy of the data-driven model, the average and maximum errors in different scenarios are presented in Table I. The results demonstrate the accuracy and practical value of the Koopman-operator-theory-based state space transformation.

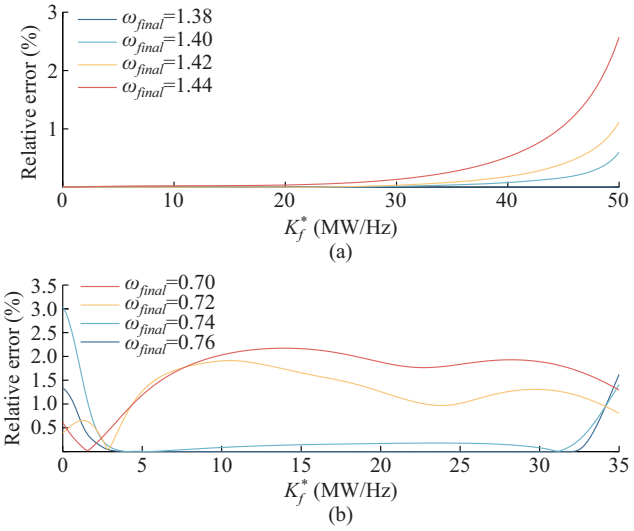

Fig. 6. Relative errors of droop coefficient. (a) Frequency-rising scenario. (b) Frequency-dropping scenario.

TABLE I
AVERAGE AND MAXIMUM ERRORS FOR FREQUENCY-RISING AND FREQUENCY-DROPPING SCENARIOS

Scenario	ω_{final} (p.u.)	Average error (%)	Maximum error (%)
Frequency-rising	1.38	0.000467	0.00140
	1.40	0.053100	0.59900
	1.42	0.118000	1.11000
	1.44	0.325000	2.57000
Frequency-dropping	0.76	0.106000	1.62000
	0.74	0.278000	3.04000
	0.72	1.270000	1.91000
	0.70	1.670000	2.17000

To verify that the proposed method is not affected by the accuracy of wind farm parameters, random errors are added to relevant parameters, for example, a −5% deviation in R and a −10% deviation in J_c. The dynamic process under the time-domain simulation without parameter errors is used as the basis for comparison. We assume that $K_{f,\max} = 20$ MW/Hz and $v = 9.2$ m/s are calculated using the dimension-augmented correlation model in a frequency-dropping scenario. When the system frequency decreases, the WTs must release rotor kinetic energy to compensate for the power shortage and participate in the PFR. The evaluation results obtained from different methods are incorporated into the PFR simulation model, and the dynamic PFR process is illustrated in Fig. 7. It can be observed that the dynamic curves of rotor speed, system frequency, and wind farm power under the proposed method are almost completely consistent with those of the time-domain simulation. In contrast, inaccurate model parameters in the time-domain simulation lead to exceeding speed limits or conservative results, indicating the advantage of the proposed method in terms of resistance to parameter errors.

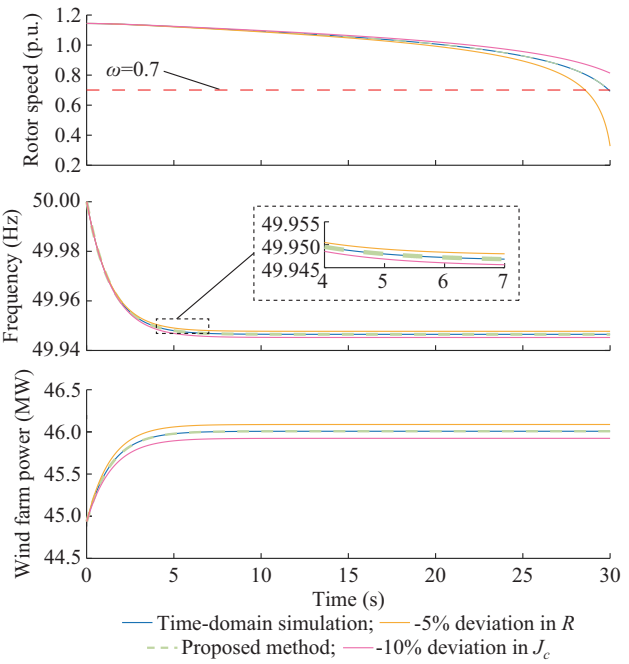

Fig. 7. Dynamic PFR process in frequency-dropping scenario.

B. PFR Capability Forecast Under Uncertain Wind Speed

By using the linear relationship matrix $\boldsymbol{M}$ to construct an equivalent linear relationship between the wind speed and the droop coefficient in an offline training manner, an online forecast of the PFR capability can be performed. Depending on the expected final rotor speed, different probability distributions of K_f^* can be derived based on the wind speed forecast. According to the PDF of the wind speed corresponding to time period t_1, the PDF of droop coefficient K_f^* in the frequency-rising and frequency-dropping scenarios is shown in Fig. 8.

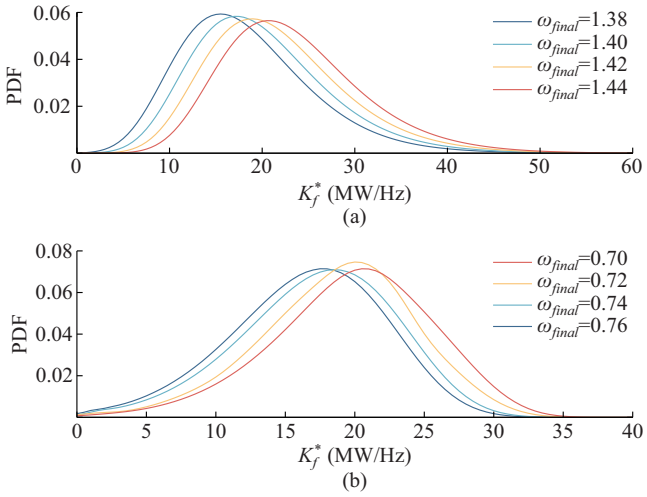

Fig. 8. PDF of droop coefficient K_f^*. (a) Frequency-rising scenario. (b) Frequency-dropping scenario.

As mentioned previously, the expected final rotor speeds for frequency-rising scenarios are 1.38 p.u., 1.40 p.u., 1.42 p.u., and 1.44 p.u., respectively, and the PDF of K_f^* corresponding to $\omega_{final}=1.44$ p.u. represents the maximum PFR capability forecast. Similarly, in the frequency-dropping scenario, the PDF of K_f^* corresponding to $\omega_{final}=0.7$ p.u. represents the maximum PFR capability forecast. As shown in Fig. 8, as ω_{final} approaches ω_{lim}, the PDF curve of K_f^* shifts further to the right, indicating that the droop coefficient increases.

Based on the PDF of K_f^* at different expected final rotor speeds, an upper confidence interval with the α quantile, denoted as $K_{f,\alpha}^*$, can be derived. For example, the upper confidence interval with the 90% quantile is listed in Table II. It can be concluded that, when ω_{final} approaches ω_{lim}, the PFR capability of wind farms is more sufficiently exploited, and a larger $K_{f,90\%}^*$ can be provided.

TABLE II
UPPER CONFIDENCE INTERVAL WITH 90% QUANTILE

Scenario	ω_{final} (p.u.)	$K_{f,90\%}^*$ (MW/Hz)
Frequency-rising	1.38	9.765
	1.40	11.313
	1.42	12.895
	1.44	14.551
Frequency-dropping	0.76	8.943
	0.74	9.704
	0.72	11.275
	0.70	12.073

The probability distribution of the maximum droop coefficient $K_{f,\max}$ corresponding to time periods t_2, t_3, and t_4 can also be derived based on the uncertain wind speed forecast shown in Fig. 5, which is illustrated in Fig. 9. The results illustrate that, when the probability distribution of wind speed moves to the right, the PFR capability tends to move in the opposite direction in the frequency-rising scenario. In contrast, the PFR capability moves to the right in the frequency-dropping scenario. These results are consistent with the monotonic relationship between the droop coefficient of the wind farm and the wind speed, as shown in Fig. 2.

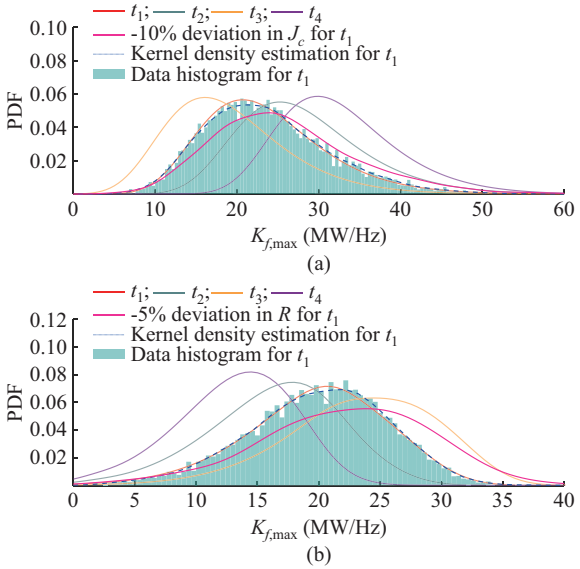

Fig. 9. PDF of maximum droop coefficient $K_{f,\max}$. (a) Frequency-rising scenario. (b) Frequency-dropping scenario.

To verify the accuracy of the probabilistic forecast, the statistical histogram of $K_{f,\max}$ obtained using simulation the time-domain simulation combined with the Monte Carlo method for time period t_1 is also provided in Fig. 9, and the corresponding PDF is obtained based on the kernel density estimation. It can be observed that the kernel density estimation results are highly consistent with those of the proposed method, demonstrating the accuracy of the proposed method. By contrast, with parameter errors in the wind farm dynamic model, time-domain simulations inevitably lead to inaccurate predictions. The pink curve in Fig. 9 represents the kernel density estimation of $K_{f,\max}$ obtained using the time-domain simulation with a −10% deviation in J_c. It is evident that the result deviates from the original curve.

In addition, when a time-domain simulation is employed combined with the Monte Carlo simulation method, the PDF of the PFR capability is not directly derived using an analytical method. Instead, it is obtained using a statistical method that is necessarily affected by random sampling errors. Theoretically, Monte Carlo simulations can produce more accurate results with more sampling points. However, the computational time also increases significantly. In this study, the Monte Carlo simulation results obtained from 10000 groups of sampling points are used as the benchmark. The upper confidence intervals with the 90% quantile $K_{f,\max,90\%}$ obtained by the Monte Carlo simulation and the proposed method and the relative errors are shown in Table III, where methods 1, 2, and 3 represent the Monte Carlo simulation with 10000, 1000, and 100 groups of sampling points, respectively.

TABLE III
UPPER CONFIDENCE INTERVALS WITH 90% QUANTILE OBTAINED BY MONTE CARLO SIMULATION AND PROPOSED METHOD AND RELATIVE ERRORS

Scenario	Time period	$K_{f,\max,90\%}$ of method 1 (MW/HZ)	Proposed method		Method 2		Method 3	
			$K_{f,\max,90\%}$ (MW/HZ)	Relative error (%)	$K_{f,\max,90\%}$ (MW/HZ)	Relative error (%)	$K_{f,\max,90\%}$ (MW/HZ)	Relative error (%)
Frequency-rising	t_1	14.578	14.551	–0.19	14.135	–3.04	13.934	–4.41
	t_2	18.841	18.862	0.11	18.414	–2.57	18.086	–4.01
	t_3	10.219	10.243	0.24	10.514	2.89	9.696	–5.12
	t_4	23.827	23.930	0.43	24.618	3.32	25.145	5.53
Frequency-dropping	t_1	11.951	12.073	1.01	11.358	–4.97	10.077	–15.68
	t_2	8.791	8.879	1.23	9.206	4.73	9.932	12.98
	t_3	15.257	15.406	0.98	16.037	5.13	17.902	17.34
	t_4	6.286	6.330	0.71	6.078	–3.31	6.924	10.16

The results suggest that, without adequate samples in the time-domain simulation, the forecast error is a challenging problem, whereas the proposed method can achieve highly accurate results (relative errors of less than 1.23%) without any sampling or dynamic simulation. The proposed method only needs to train the dimension-augmented correlation model in advance to realize the real-time forecasting of the PFR capability based on wind speed probability. In contrast, if a statistical method is used, the time cost of sampling and simulation exhibits an extraordinarily increasing trend. The computational time for the Monte Carlo simulation and the proposed method is shown in Table IV.

TABLE IV
COMPUTATIONAL TIME FOR MONTE CARLO SIMULATION AND PROPOSED METHOD

Scenario	Time period	Computational time (s)			
		Method 1	Proposed method	Method 2	Method 3
Frequency-rising	t_1	19360	0.223	1947	194.539
	t_2	19490	0.209	1939	194.992
	t_3	19480	0.212	1923	194.441
	t_4	19240	0.302	1928	194.717
Frequency-dropping	t_1	19290	0.201	1904	192.911
	t_2	19190	0.207	1913	192.871
	t_3	19010	0.206	1927	191.456
	t_4	19260	0.198	1922	192.400

The results validate that the proposed method has a significant advantage in terms of computational time compared with the Monte Carlo simulation, and a five-order-of-magnitude reduction in computational time makes online prediction feasible.

Note that the droop coefficient distribution obtained by the Monte Carlo simulation is based on random sampling from the Weibull distribution of wind speed. When the number of sample points is small, random sampling errors may be significant, causing the sample points to represent the characteristics of the wind speed based on Weibull distribution inaccurately. This, in turn, can result in an unreasonable probability distribution of the droop coefficient. Taking the wind speed distribution during period t_1 as an example, we present the probability distribution curves of $K_{f,\max}$ obtained from the Monte Carlo simulation with three sets of 100 groups of sample points (sets A, B, and C) in both frequency-rising and frequency-dropping scenarios. As shown in Fig. 10, when the number of groups of sample points is small, the PDF of $K_{f,\max}$ obtained using statistical methods may deviate significantly from the true distribution curve. The proposed method addresses this issue effectively.

C. Discussion on Probabilistic Forecast

Note that, owing to the probability distribution of the PFR capability that it can provide, the probabilistic forecast plays an important role in scheduling the frequency regulation resources for power systems.

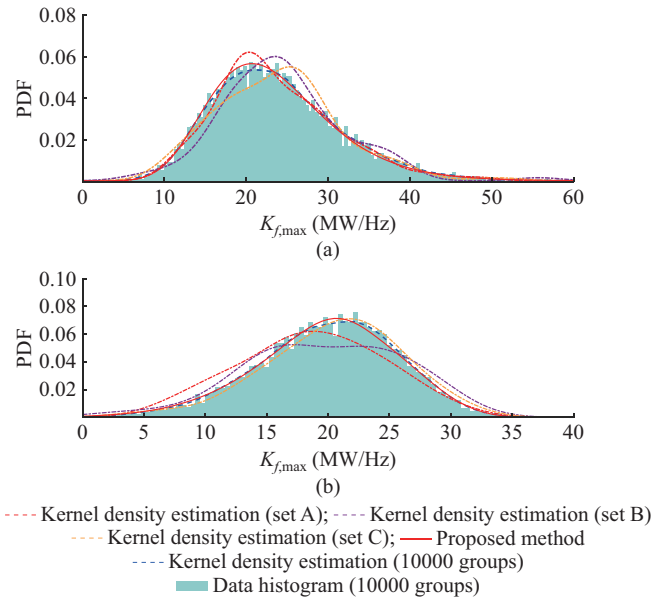

Fig. 10. PDF of $K_{f,\max}$ obtained from Monte Carlo simulation and proposed method. (a) Frequency-rising scenario. (b) Frequency-dropping scenario.

Compared with simple point forecasts, probabilistic forecasts contain comprehensive information and, hence, may reach different conclusions. We take frequency-rising scenarios as examples to explain the importance of probabilistic forecast. As shown in Fig. 11, when point forecast is used, the wind speeds are 9.2409 m/s and 8.3652 m/s for scenarios 1 and 2, respectively.

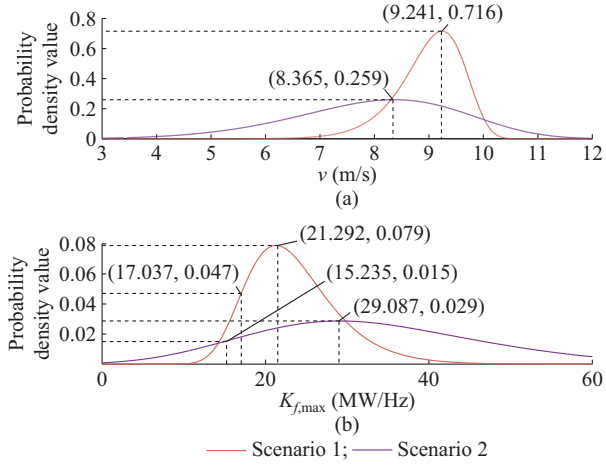

Fig. 11. Comparison of point forecast and probabilistic forecast. (a) Result of wind speed. (b) Result of PFR capability.

According to the point forecast, $K_{f,\max}$ is computed, and the result is 21.2918 MW/Hz in scenario 1 and 29.0867 MW/Hz in scenario 2, respectively. The point forecast result of PFR capability in scenario 1 is smaller than that in scenario 2, respectively, which is consistent with our intuitive understanding. Nevertheless, the probabilistic forecast results of $K_{f,\max,90\%}$ are 17.0366 MW/Hz in scenario 1 and 15.2348 MW/Hz in scenario 2, respectively. An interesting conclusion can be drawn: scenario 1 has a larger $K_{f,\max,90\%}$ than scenario 2, as shown in Fig. 11(b), which exhibits the trend opposite to the point forecast.

Figure 11 shows the significance of the probabilistic forecast over point or interval forecasts. As the PDF of $K_{f,\max}$ can be obtained using the proposed method, the confidence interval for any confidence level can be easily calculated according to the function, illustrating the superiority of the physics-informed scheme.

VI. Conclusion

The increasing penetration of wind power generation has necessitated PFR capability forecast for wind farms based on wind speed distribution. This paper proposes a physics-informed probability distribution assessment method for the PFR capability of wind farms that considers wind speed uncertainty. By employing historical data of the PFR capability of wind farms, a dimension-augmented correlation model of the wind speed, rotor speed, and droop coefficient is constructed. Based on the probability distribution of the predicted wind speed, the PDF of the PFR capability, that is, the maximum droop coefficient of the wind farm, is derived. The simulation results validate that, compared with the traditional time-domain simulation combined with the Monte Carlo simulation method, the proposed method can directly obtain an analytical expression for the probability distribution of the PFR capability without historical data covering all extreme scenarios. A more prominent advantage is the computational time, which is reduced by five orders of magnitude using the proposed method to realize similar accuracy, which makes it suitable for online applications. In addition, probabilistic forecasts reflect more comprehensive information than traditional point forecasts, which is conducive for scheduling a reliable plan for the dynamic dispatching of frequency regulation resources.

References

[1] J. Morren, S. W. H. de Haan, W. L. Kling *et al*., "Wind turbines emulating inertia and supporting primary frequency control," *IEEE Transactions on Power Systems*, vol. 21, no. 1, pp. 433-434, Feb. 2006.

[2] Q. Hou, E. Du, N. Zhang *et al*., "Impact of high renewable penetration on the power system operation mode: a data-driven approach," *IEEE Transactions on Power Systems*, vol. 35, no. 1, pp. 731-741, Jan. 2020.

[3] W. Tang, J. Hu, Y. Chang *et al*., "Modeling of DFIG-based wind turbine for power system transient response analysis in rotor speed control timescale," *IEEE Transactions on Power Systems*, vol. 33, no. 6, pp. 6795-6805, Nov. 2018.

[4] D. Ochoa and S. Martinez, "Fast-frequency response provided by DFIG-wind turbines and its impact on the grid," *IEEE Transactions on Power Systems*, vol. 32, no. 5, pp. 4002-4011, Sept. 2017.

[5] M. Yin, Y. Xu, C. Shen *et al*., "Turbine stability-constrained available wind power of variable speed wind turbines for active power control," *IEEE Transactions on Power Systems*, vol. 32, no. 3, pp. 2487-2488, May 2017.

[6] V. Prakash, K. Sharma, R. Bhakar *et al*., "Frequency response constrained modified interval scheduling under wind uncertainty," *IEEE Transactions on Sustainable Energy*, vol. 9, no. 1, pp. 302-310, Jan. 2018.

[7] M. H. Athari and Z. Wang, "Impacts of wind power uncertainty on grid vulnerability to cascading overload failures," *IEEE Transactions on Sustainable Energy*, vol. 9, no. 1, pp. 128-137, Jan. 2018.

[8] X. Xi, H. Geng, G. Yang *et al*., "Torsional oscillation damping control for DFIG-based wind farm participating in power system frequency regulation," *IEEE Transactions on Industry Applications*, vol. 54, no. 4, pp. 3687-3701, Jul. 2018.

[9] S. de Rijcke, P. Tielens, B. Rawn *et al*., "Trading energy yield for fre-

quency regulation: optimal control of kinetic energy in wind farms," *IEEE Transactions on Power Systems*, vol. 30, no. 5, pp. 2469-2478, Sept. 2015.
[10] H. Ye, W. Pei, and Z. Qi, "Analytical modeling of inertial and droop responses from a wind farm for short-term frequency regulation in power systems," *IEEE Transactions on Power Systems*, vol. 31, no. 5, pp. 3414-3423, Sept. 2016.
[11] A. D. Hansen, P. Sørensen, F. Iov *et al*., "Centralised power control of wind farm with doubly fed induction generators," *Renewable Energy*, vol. 31, no. 7, pp. 935-951, Jun. 2006.
[12] M. Kayikci and J. V. Milanovic, "Dynamic contribution of DFIG-based wind plants to system frequency disturbances," *IEEE Transactions on Power Systems*, vol. 24, no. 2, pp. 859-867, May 2009.
[13] Z. Wang and W. Wu, "Coordinated control method for DFIG-based wind farm to provide primary frequency regulation service," *IEEE Transactions on Power Systems*, vol. 33, no. 3, pp. 2644-2659, May 2018.
[14] L. Guo, Y. Ren, Z. Wang *et al*., "Double-layer feedback control method for synchronized frequency regulation of PMSG-based wind farm," *IEEE Transactions on Sustainable Energy*, vol. 12, no. 4, pp. 2423-2435, Oct. 2021.
[15] Z. Wang, J. Liu, L. Guo *et al*., "Droop-inertia frequency regulation feasible region assessment for wind farm based on data-driven state space mapping," *IEEE Transactions on Industry Applications*, vol. 61, no. 1, pp. 1704-1715, Jan.-Feb. 2025.
[16] L. Wu, "A tighter piecewise linear approximation of quadratic cost curves for unit commitment problems," *IEEE Transactions on Power Systems*, vol. 26, no. 4, pp. 2581-2583, Nov. 2011.
[17] E. Du, N. Zhang, C. Kang *et al*., "A high-efficiency network-constrained clustered unit commitment model for power system planning studies," *IEEE Transactions on Power Systems*, vol. 34, no. 4, pp. 2498-2508, Jul. 2019.
[18] V. Gevorgian, Y. Zhang, and E. Ela, "Investigating the impacts of wind generation participation in interconnection frequency response," *IEEE Transactions on Sustainable Energy*, vol. 6, no. 3, pp. 1004-1012, Jul. 2015.
[19] Z. Zhang, E. Du, F. Teng *et al*., "Modeling frequency dynamics in unit commitment with a high share of renewable energy," *IEEE Transactions on Power Systems*, vol. 35, no. 6, pp. 4383-4395, Nov. 2020.
[20] K. V. Vidyanandan and N. Senroy, "Primary frequency regulation by deloaded wind turbines using variable droop," *IEEE Transactions on Power Systems*, vol. 28, no. 2, pp. 837-846, May 2013.
[21] P. Kou, D. Liang, L. Yu *et al*., "Nonlinear model predictive control of wind farm for system frequency support," *IEEE Transactions on Power Systems*, vol. 34, no. 5, pp. 3547-3561, Sept. 2019.
[22] M. Kheshti, L. Ding, W. Bao *et al*., "Toward intelligent inertial frequency participation of wind farms for the grid frequency control," *IEEE Transactions on Industrial Informatics*, vol. 16, no. 11, pp. 6772-6786, Nov. 2020.
[23] Y. Liang, X. Zhao, and L. Sun, "A multiagent reinforcement learning approach for wind farm frequency control," *IEEE Transactions on Industrial Informatics*, vol. 19, no. 2, pp. 1725-1734, Feb. 2023.
[24] J. Liu, Z. Wang, X. Zang *et al*, "Data-driven dynamic assessment method of wind farm frequency characteristics based on state space mapping," *CSEE Journal of Power and Energy Systems*, vol. 11, no. 3, pp. 1018-1029, May 2025.
[25] J. Shi, Z. Ding, W. J. Lee *et al*., "Hybrid forecasting model for very-short term wind power forecasting based on grey relational analysis and wind speed distribution features," *IEEE Transactions on Smart Grid*, vol. 5, no. 1, pp. 521-526, Jan. 2014.
[26] Z. Wang and S. Bu, "Generic multi-output spectral representation method for uncertainty propagation analysis of power system dynamics," *Journal of Modern Power Systems and Clean Energy*, vol. 13, no. 3, pp. 757-765, May 2025.
[27] M. Dadkhah and B. Venkatesh, "Cumulant based stochastic reactive power planning method for distribution systems with wind generators," *IEEE Transactions on Power Systems*, vol. 27, no. 4, pp. 2351-2359, Nov. 2012.
[28] T.-H. Yeh and L. Wang, "A study on generator capacity for wind turbines under various tower heights and rated wind speeds using Weibull distribution," *IEEE Transactions on Energy Conversion*, vol. 23, no. 2, pp. 592-602, Jun. 2008.
[29] M. He, L. Yang, J. Zhang *et al*., "A spatio-temporal analysis approach for short-term forecast of wind farm generation," *IEEE Transactions on Power Systems*, vol. 29, no. 4, pp. 1611-1622, Jul. 2014.
[30] J. L. Proctor, S. L. Brunton, and J. N. Kutz, "Generalizing Koopman theory to allow for inputs and control," *SIAM Journal on Applied Dynamical Systems*, vol. 17, no. 1, pp. 909-930, Jan. 2018.
[31] L. Guo, Y. Zhang, X. Li *et al*., "Data-driven power flow calculation method: a lifting dimension linear regression approach," *IEEE Transactions on Power Systems*, vol. 37, no. 3, pp. 1798-1808, May 2022.
[32] Y. Xu, Q. Wang, L. Mili *et al*., "A data-driven Koopman approach for power system nonlinear dynamic observability analysis," *IEEE Transactions on Power Systems*, vol. 39, no. 2, pp. 4090-4104, Mar. 2024.

Wenlong Wu received the B.S. degree in electrical engineering from Hebei University of Technology, Tianjin, China, in 2023. He is currently working toward the M.Sc. degree with Tianjin University. His research focuses on assessment of renewable power generation.

Zhongguan Wang received the B.S. and Ph.D. degrees from the Department of Electrical Engineering, Tsinghua University, Beijing, China, in 2014 and 2019, respectively. He is currently an Associate Professor with the School of Electrical and Information Engineering, Tianjin University, Tianjin, China. His research interests include operation of renewable power generation and energy management for active distribution network.

Xialin Li received the B.Sc. and Ph.D. degrees from Tianjin University, Tianjin, China, in 2009 and 2014, respectively. In 2016, under the State Scholarship Fund, he was a Visiting Professor with the Department of Electrical and Computer Engineering, University of Alberta, Edmonton, Canada. Since 2018, he has been an Associate Professor with the School of Electrical Engineering and Automation, Tianjin University. His research interests include modeling and control of power converters, distributed generation, hybrid AC-DC microgrid, and multiterminal DC (MTDC) grid.

Li Guo received the B.S. and Ph.D. degrees in electrical engineering from the South China University of Technology, Guangzhou, China, in 2002 and 2007, respectively. He is currently a Full Professor with Tianjin University, Tianjin, China. His research interests include optimal planning and design of microgrid, coordinated operating strategy of microgrid, and advanced energy management system.

Yixin Liu received the B.S. and Ph.D. degrees in electrical engineering from Tianjin University, Tianjin, China, in 2013 and 2018, respectively. He is currently an Associate Professor with Tianjin University. His research interests include transient stability analysis control in AC power system, analysis and planning of distribution system, energy management for microgrid, and electricity market.

Jiaqing Zhai received the B.S. degree in electrical engineering from Yanshan University, Qinhuangdao, China, in 2022. In the same year, he began the master's studies with Tianjin University, Tianjin, China. In 2024, he transitioned to a combined master's and Ph.D. program and is currently working toward the Ph.D. degree in electrical engineering with Tianjin University. His research focuses on control and scheduling of renewable energy generation.

Chengshan Wang received the Ph.D. degree in electrical engineering from Tianjin University, Tianjin, China, in 1991. From 1994 to 1996, he was a Senior Academic Visitor with Cornell University, Ithaca, USA. From 2001 to 2002, he was a Visiting Professor with Carnegie Mellon University, Pittsburgh, USA. He is currently a Professor with the School of Electrical Engineering and Automation, Tianjin University, where he is also the Director of the Key Laboratory of Smart Grid of Ministry of Education. His research interests include distribution system analysis and planning, distributed generation system, microgrid, and security analysis of power system.